# Development of a 0.1 kW power accumulation pilot plant based on an Fe/Cr redox flow battery Part 1. Considerations on flow-distribution design

G. Codina, J.R. Perez, M. Lopez-Atalaya, J.L. Vazquez and A. Aldaz*
*Departamento Química Física, Universidad de Alicante, Apartado 99, 03080 Alicante (Spain)*

(Received July 23, 1993; accepted September 11, 1993)

**Abstract**

The design of a flow-distribution system for a 0.1 kW Fe/Cr redox flow battery has been based on the application of shunt current calculation model to a 20-cell bipolar system. A model to simulate the intra-stack flow distribution has also been proposed. Both shunt-current and flow-distribution analysis have yielded a prototype with a 93% current efficiency with an homogeneous intrastack flow distribution.

## Introduction

The concept of a redox flow battery as an energy bulk accumulation system is based on the storage of two fully soluble redox couples which are continuously pumped through a power conversion cell. Due to this feature, the energy storage capacity and the power of this kind of systems are able to be independently sized. Therefore, these systems are suitable for their use in load-leveling and stand-alone applications [1, 2]. A basic cell consists of two inert electrodes separated by an ion-exchange membrane. From the previous studies developed, the electrolytes selected were two identical solutions for both half-cells (1.25 M $CrCl_3$+1.25 M $FeCl_2$+2.3 M HCl) [3, 4].

During battery operation, hydrogen evolution has been reported as a competitive process to Cr(III) ion reduction that produces a decrease in the coulombic efficiency [5, 6]. To avoid this evolution, $PbCl_2$ was added to both electrolytes in agreement with the results reported on the Cr(III)/Cr(II) couple electrocatalysis on carbonaceous electrodes [4, 6, 7].

The transmission of electric energy has a higher energy efficiency when it is performed by high voltage/low current devices than when it is performed by low voltage/high current ones. For this reason, batteries arranged in bipolar assemblies are preferred to monopolar ones. When these bipolar systems have a common electrolyte, as it is in the case of redox flow batteries, shunt currents appear due to the electrolyte connections between electrodes.

Thus, a fraction of the energy provided to the system is shunted through these electrolyte paths, not being used by the electrochemical process, and producing a decrease in the energy efficiency. Moreover, other undesirable processes induced by these shunt currents, as electrode corrosion and gas evolution, must be pointed out.

*Author to whom correspondence should be addressed.


*SSDI* 0378-7753(93)01846-A

Shunt current analysis has been carried out by several authors by applying Kirchhoff's laws to electrical circuit analogs of an stack of cells [8–13]. The procedures to decrease shunt currents usually originate in an increase of pump-power losses.

The internal electrolyte flow distribution is determined by the relationship between the hydraulic resistance of the electrode flow distributor system and the manifold. Previous work released by Hagedorn *et al.* [14] revealed that, when this relationship is small, extreme cells of the stack work with flows higher than the stack average flow, while the central cells work with lower ones. This effect begins to be more significant when the stack average flow is close to the stoichiometric flow, due to the appearance of diffusion overvoltage.

The aim of this paper is to obtain a suitable cell design in order to minimize energy losses due to shunt currents and pumping power in a 0.1 kW Fe/Cr redox flow battery. A model to evaluate the intra-stack flow distribution has also been proposed.

## Simulation models

*Shunt-current analysis*

In Fig. 1, a diagram of a single-stack redox flow cell (a) and its analog circuit (b) is shown. The different components are represented as follows: $R_i$, internal cell resistance; $V_o$, open-circuit cell voltage; $R_c$, port feed and exit resistance; $R_m$, manifold segment resistance, and $I_t$, charge/discharge current. Each cell, except the two terminal ones, generates four independent current loops, these loops having their own cell as a common element. Terminal cells only generate two current loops due to the fact that the electrolyte network is assumed to be interrupted at the pumping section. Thus, the circuit proposed above is defined by a set of $4N-4$ (where $N$ is the number of cells of the stack) loop currents that must satisfy the same number of Kirchhoff's equations (1):

$$\sum_{j}^{p} i_j R_j - V_o = 0 \tag{1}$$

where $p$ is the number of resistors in each loop. Real currents $i_j$ can be calculated as a function of loop currents, $I_k$, using eqn. (2):

$$i_j = \sum_{k}^{q} I_k \tag{2}$$

where $q$ is the number of loop currents in each circuit branch. The value of each equivalent resistor $R_j$ may be calculated using eqn. (3):

$$R_i = \rho_i \frac{l_i}{S_i} \tag{3}$$

where $\rho_i$ is the specific resistivity of the electrolyte; $l_i$ is the pipe length, and $S_i$ is its cross-sectional area.

The shunt current is defined as the difference between the total current $I_t$ and the real current $i_j$ circulating through each cell. More information on this simulation model is available in the literature cited [8–13]. The mathematical resolution of this equation system was carried out using the software developed in our laboratory based on the simple iteration method [15]. The voltage efficiency was directly calculated by

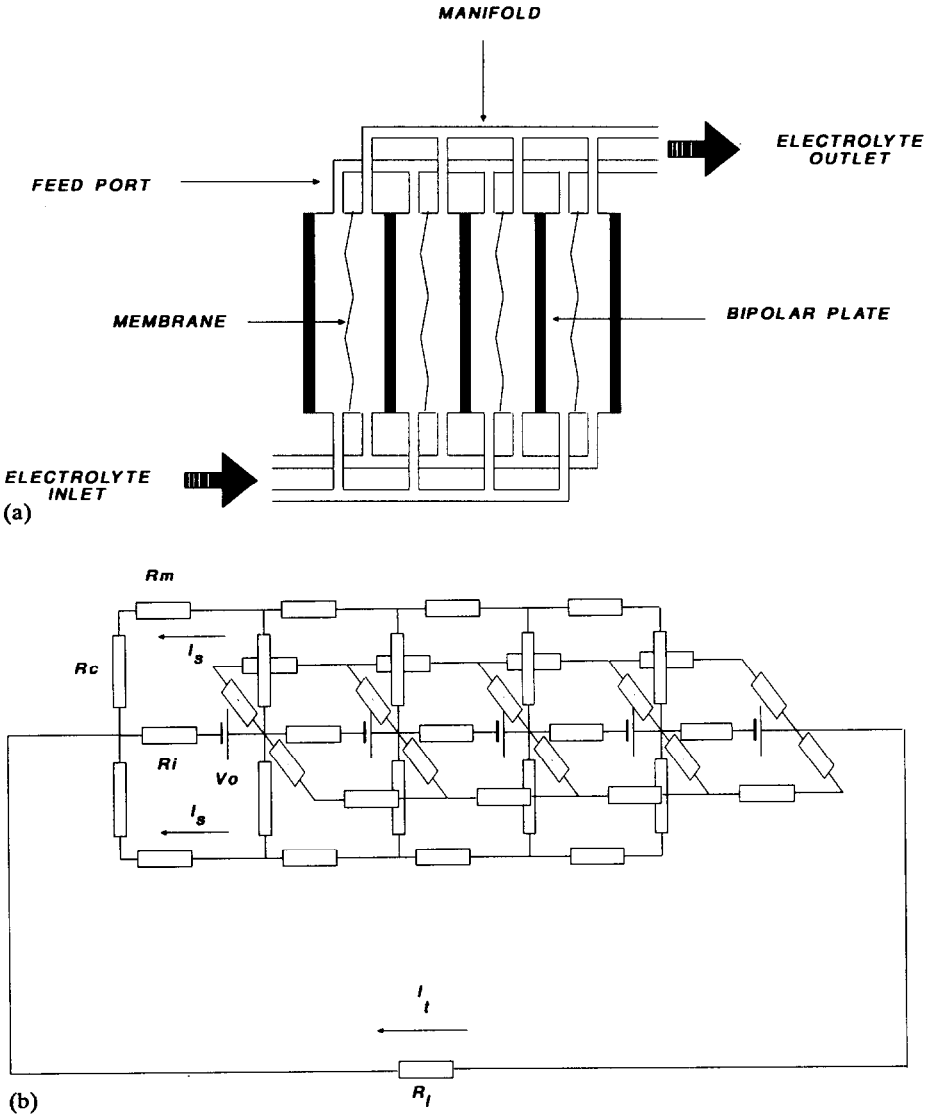


Fig. 1. (a) Schematic of redox flow cell; (b) circuit analog.

the ratio between the battery voltages in discharge and charge operation, using as $V_o$ the open-circuit cell voltage at 50% state-of-charge. The current efficiency has been calculated with eqn. (4):

$$\eta_c = 1 - \frac{\sum_{i=1}^{N}(I^c_{s,i} + I^d_{s,i})}{NI_t} \tag{4}$$

where $I^c_{s,i}$ and $I^d_{s,i}$ represent shunt current at cell $i$ during charge and discharge operation, respectively. Energy efficiency has been calculated as the product of voltage and current efficiencies.

*Flow-distribution analysis*

A scheme of the internal flow distribution in a redox flow cell is shown in Fig. 2. The pressure drop generated when a solution flows through a hydraulic circuit element with a constant cross-sectional area can be calculated making a mechanical energy balance (eqn. (5)):

$$\frac{\Delta P}{\rho} + g\Delta z = \hat{W} - \frac{2fl\langle v\rangle^2}{d} \tag{5}$$

where $\Delta P$ is the pressure drop, $\rho$ the electrolyte density, $\Delta z$ the unevenness of the element, $g$ the gravity constant, $\langle v\rangle$ the average flow speed, $f$ the friction factor, $l$ the equivalent length of the element, $d$ its equivalent diameter, and $\hat{W}$ the energy per mass unit applied.

In a general way, the pressure drop may be evaluated in terms of equivalent hydraulic resistors and flows (eqn. (6)):

$$\Delta P = R_i(Q_i)Q_i \tag{6}$$

The model proposed is based on the application of eqns. (5) and (6) of a hydraulic circuit analog of a stack of cells. In Fig. 3, the hydraulic circuit analog to a half-stack formed by five cells has been represented. The various components of the circuit are represented as follows: $R_c$, cell equivalent resistor; $R_m$, manifold equivalent resistor, and $Q_t$, total electrolyte flow. Thus, the circuit described is defined by a set of $N$–1 equations:

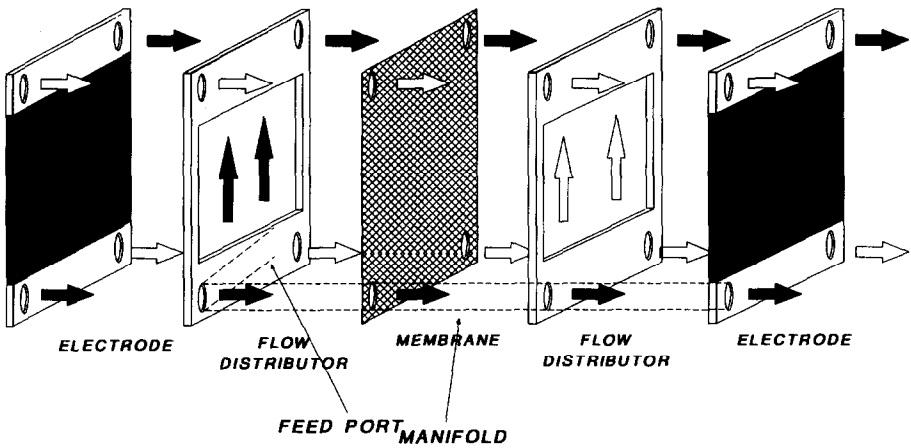


Fig. 2. Schematic of the internal flow distribution in a redox flow cell.

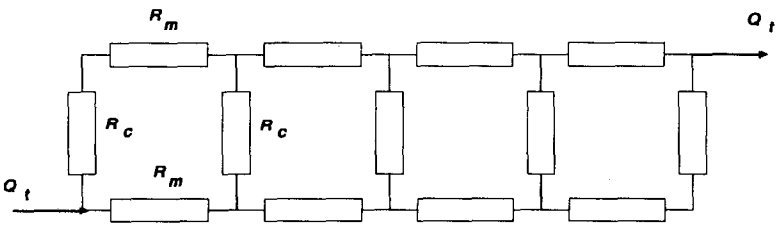


Fig. 3. Hydraulic circuit analog of a non-divided redox flow cell.

$$\Delta P - \sum_j R_j q_j = 0 \tag{7}$$

The real flow of electrolyte $q_j$ in each circuit branch can be calculated from the loop flows $Q_k$:

$$q_j = \sum_k Q_k \tag{8}$$

The $R_j$ values are calculated by the following set of equations:

$$R_{mj} = \frac{2\rho_j l_j q_j f_j}{d_j s_j^2} \tag{9}$$

$$R_{cj} = \frac{4\rho_j l_j q_j f_j}{d_j s_j^2} + k + \frac{\rho_j g \Delta z}{q_j} \tag{10}$$

where $k$ is the Kozney–Karman constant [16]. The $f_j$ value can be calculated from the corresponding Reynolds module. Since the $R_j$ values depend on the corresponding flow $q_j$, the equations must be solved using an iterative method.

## Results and discussion

*Shunt-current analysis*

The design parameters of a 0.1 kW battery are shown in Table 1. The evolution of battery efficiency as a function of the number of cells of the stack has been represented in Fig. 4. Voltage efficiency shows no significant variations when the number of cells increases. This is due to the low voltage drops produced by the internal cell resistance compared with the open-circuit cell voltage. Logically, current efficiency decreases with the number of cells as a consequence of the increase in the shunt

TABLE 1

Nominal design specifications of a 0.1 kW Fe/Cr redox flow battery

| | |
|---|---|
| Nominal power (W) | 120 |
| Gross power (W) | 230 |
| Electrode area ($cm^2$) | 200 |
| Cell voltage (V, oc, 50% sc) | 20.6 |
| Current density ($mA/cm^2$) | 40 |
| Number of cells[a] | 21 |
| Manifold | |
| Length (cm) | 1.8 |
| Section ($cm^2$) | 1.5 |
| Feed port | |
| Length (cm) | 12 |
| Section ($cm^2$) | 0.21 |
| Electrolyte | |
| Density ($g/cm^3$) | 1.33 |
| Viscosity (g/cm) | 0.03 |
| Electrode | |
| $k$ (g/s $cm^4$)[b] | 8080 |
| $\Delta z$ (cm) | 18 |

[a]Power cells and state-of-charge measure cell.

[b]Obtained from the experimental drop-flow battery response.

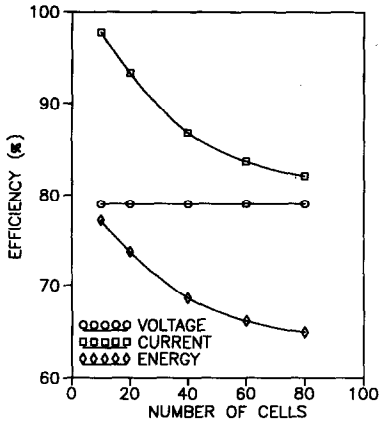


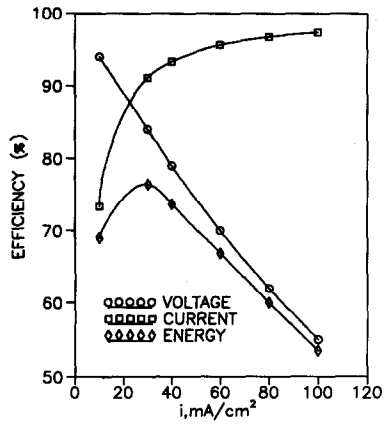


Fig. 4. Battery efficiency as a function of the number of cells. Input parameters: $R_m = 4.2\ \Omega$; $R_c = 334\ \Omega$; $V_o = 1.032$ V; $R_i = 0.015\ \Omega$; $R_m = 4.2\ \Omega$; $R_c = 334\ \Omega$, and $I_t = 8$ A.

Fig. 5. Battery efficiency as a function of the charge/discharge current density. Input parameters: $N = 20$ cells; $V_o = 1.032$ V; $R_i = 0.015\ \Omega$; $R_m = 4.2\ \Omega$, and $R_c = 334\ \Omega$.

currents. Since voltage efficiency stays constant in the range studied, the variation of energy efficiency is similar to that presented by current efficiency. From these results, it can be concluded that it may be not suitable to built stacks with over 30 cells to yield energy efficiencies over 70%. However, it power demand rises, this battery would be able to work with a number of cells close to 80 with an energy efficiency of more than 65%.

In Fig. 5, the battery efficiency as a function of charge/discharge current density has been represented. The increase of the charge/discharge current provides a logical decrease of the voltage efficiency. However, this increase of the charge/discharge current generates an increase in the current efficiency. This fact is in agreement with the behaviour presented by the shunt current when the charge/discharge current is increased [8, 9]. As a direct consequence of the inverse response presented by the voltage and current efficiencies when the total current increases, energy efficiency reaches a maximum at a current density around 30 mA/cm$^2$. From these results, it can be concluded that energy efficiencies over 70% may be reached working with current densities close to 10 mA/cm$^2$. If power demand increases, the designed battery could work at a charge/discharge current density of 70 mA/cm$^2$ with an energy efficiency close to 65%.

The internal cell resistance is determined by the following factors: (i) electrolyte specific resistivity; (ii) flow distributor geometry, (iii) and current collector/electrode contact resistance. In Fig. 6, a study of the influence of the internal cell resistance on battery efficiency is shown. Obviously, a diminution of the internal cell resistance will not appreciably affect to the coulombic efficiency because the variation of the cell voltage induced by the decrease in the internal resistance is so small that the increase in shunt current in each cell may be neglected. However, the energetic efficiency rises when the internal cell resistance diminishes, due to the increase in the voltage efficiency. From these results, energy efficiencies more than 85% may be expected, if the internal cell resistance decreases to values close to 1 $\Omega$ cm$^2$.

The influence of manifold and port cross-sectional area has also been studied (Fig. 7). From these results, the electrolyte flow distribution can be designed with a

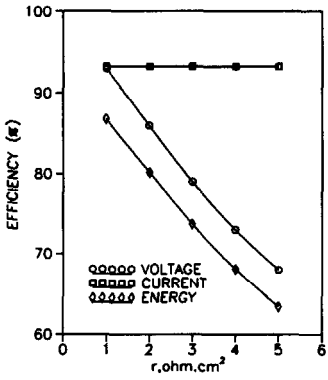


Fig. 6. Battery efficiency as a function of the internal cell resistance. Input parameters: $N=20$ cells; $V_o=1.032$ V; $R_m=4.2$ Ω; $R_c=334$ Ω and $I_t=8$ A.

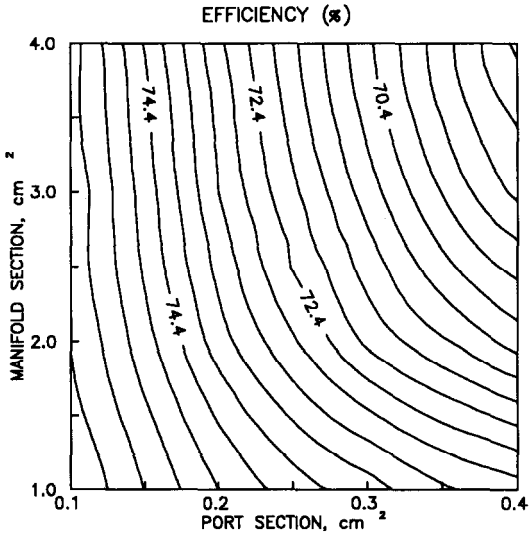


Fig. 7. Level-line diagram corresponding to the battery energy efficiency as a function of port and manifold cross section. Input parameters: $N=20$ cells; $V_o=1.032$ V; $R_i=0.015$ Ω, and $I_t=8$ A.

wide range of manifold and port cross sections with energy efficiency consistently more than 70%.

*Flow-distribution analysis*

In the model proposed above, the Kozney–Karman parameter must be calculated for our system, previous to the calculation of the intra-stack flow distribution of the battery. This parameter has been calculated from the pressure drop/flow response of the battery. The calculation algorithm is based on the optimization of the $k$ parameter by the SIMPLEX method [17, 18]. The function to be minimized is:

$$Q=\sum_i(\Delta P_{i,\,\mathrm{exp}}-\Delta P_{i,\,\mathrm{sim}})^2 \qquad (11)$$

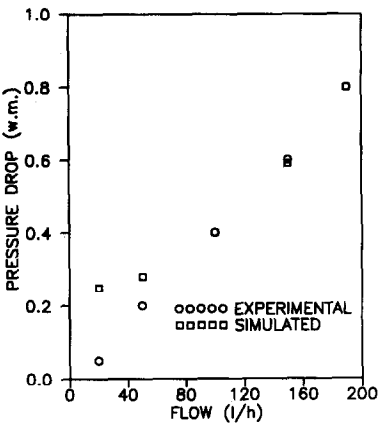


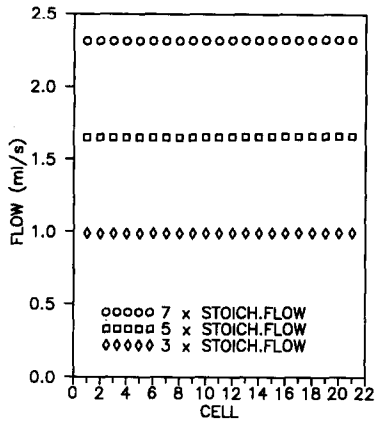


Fig. 8. Comparison between the cell pressure drop (expressed in meters of water) simulated and experimentally obtained.

Fig. 9. Simulated intra-stack flow distribution.

where $\Delta P_{i,\,exp}$ and $\Delta P_{i,\,sim}$ represent the experimental and calculated pressure drop, respectively.

From the results experimentally obtained and simulated, a suitable performance of the simulation model has been found in the flow working range of the battery (over 100 l/h). The intra-stack flow distribution for different flows has been represented in Fig. 8. From these results, a suitable intra-stack flow distribution may be expected for the proposed cell design.

## Conclusions

The design analysis of a flow distribution frame based on shunt current calculation models has yield a prototype with a theoretical current efficiency of 93% for a 20-cell battery with 200 $cm^2$ of electrode area. Moreover, the model proposed in order to simulate the intra-stack flow distribution has shown a suitable performance in the studied flow range. From the results obtained in this study, a homogeneous intra-stack flow distribution may be expected.

## Acknowledgements

This project has been financed by Iberdrola SA, SEA Tudor SA, Universidad de Alicante and EEC (through JOULE programme contract no. EC 094/88 ES). The collaboration of M.A. Pastor and J. Medina is also acknowledged.

## List of symbols

$R_i$ internal cell resistance
$V_o$ open-circuit cell voltage

$R_c$ port feed and exit resistance
$R_m$ manifold segment resistance
$I_t$ charge/discharge current
$N$ number of cells of the stack
$\rho_i$ specific resistivity of the electrolyte
$i_j$ current circulating through each circuit element
$I_k$ loop current in each circuit branch
$l_i$ circuit element length
$S_i$ circuit element cross-sectional area
$I^c_{s,i}$ shunt current at cell $i$ during charge operation
$I^d_{s,i}$ shunt current at cell $i$ during discharge operation
$\eta_c$ current efficiency
$\Delta P_j$ pressure drop through circuit element j
$\rho$ electrolyte density
$\Delta z_j$ uneveness of the hydraulic circuit element
$g$ gravity constant
$\langle v \rangle$ average flow speed
$f_j$ friction factor of circuit element $j$
$l_j$ equivalent length of circuit element $j$
$d_j$ equivalent diameter of circuit element $j$
$\dot{W}$ energy per mass unit applied
$Q_t$ total electrolyte flow
$q_j$ flow through circuit element $j$
$Q_i$ loop flow
$k$ Kozney–Karman parameter

## References


1 L.H. Thaller, *9th Intersociety Energy Conversion Engineering Conf., San Francisco, CA, USA, Aug. 26–30, 1974, NASA TM X-71540*, pp. 924–928.
2 N.H. Hagedorn, *DOE/NASA/12726-8, NASA TM-82607*, 1981.
3 D.A. Johnson and M.A. Reid, *J. Electrochem. Soc., 132* (1985) 1058.
4 M. López-Atalaya, G. Codina, J.R. Pérez, J.L. Vázquez and A. Aldaz, *J. Power Sources, 39* (1992) 147–154.
5 N.H. Hagedorn, *DOE/NASA/12726-24, NASA TM-83677*, 1984.
6 M. López-Atalaya, G. Codina, J.R. Pèrez, J.L. Vázquez and A. Aldaz, *J. Power Sources, 35* (1991) 225–234.
7 M.A. Reid, R.F. Gahn, J.S. Ling and J. Charleston, *DOE/NASA/12726-13, NASA TM-82702*, 1980.
8 E.A. Kaminski and R.F. Savinelli, *J. Electrochem. Soc., 130* (1983) 1103.
9 P.G. Grimes, R.J. Bellows and M. Zahn, in R.E. White (ed.), *Electrochemical Cell Design*, Plenum, New York, 1984, p. 259.
10 P.G. Grimes and R.J. Bellows, in R.E. White (ed.), *Electrochemical Cell Design*, Plenum, New York, 1984, p. 277.
11 J.W. Holmes and R.E. White, in R.E. White (ed.), *Electrochemical Cell Design*, Plenum, New York, 1984, p. 311.
12 R.E. White, C.W. Walton, H.S. Burney and R.W. Beaver, *J. Electrochem. Soc., 133* (1986) 485.
13 S. Szpak, C.J. Gabriel and J.R. Driscoll, *J. Electrochem. Soc., 131* (1984) 1996.
14 N.H. Hagedorn, M.A. Hoberecht and L.H. Thaller, *DOE/NASA/12726-11, NASA TM-82686*, 1982.

15 C. Froberg, *Introduction to Numerical Analysis*, Adison–Wesley, New York, 1969, p. 112.
16 K. Kanari, K. Nozaki and T. Ozawa, *AlChE Symp. Ser. Electrochemical Applications, VI, 83* (1987), p. 104.
17 P.C. Jurs, *Computer Software Applications in Chemistry*, Willey–Interscience, New York, 1986.
18 W.H. Press, B.P. Flannery, S.A. Teulkosky and W.F. Vetterling, *Numerical Recipes. Fortran Version*, Cambridge University Press, Cambridge, 1989.